Optimal Power Control of Hybrid PEM Fuel Cell Systems for an Accelerated System Warm-up

Eric A. Müller, Anna G. Stefanopoulou, *Member, IEEE,* and Lino Guzzella, *Senior Member, IEEE*

***Abstract*— Power management and thermal control are key technical challenges in fuel cell power system applications. In this paper, an optimal supervisory controller for the operation of a hybrid polymer electrolyte membrane (PEM) fuel cell power system equipped with an auxiliary coolant heater is presented. This predictive feedback controller is designed to minimize the transient warm-up phase after a cold start. It drives the system to its operating temperature within minimal time while taking into account certain energy and temperature constraints. To this end, a control-oriented mathematical model of the system is developed and partially validated with experimental data. The proper operation of the controller is verified for various operating conditions. Compared to a system without battery nor auxiliary heater, the simulation shows a significantly reduced warm-up time for the optimally controlled configuration proposed.**

***Index Terms*— PEM fuel cell system, hybridization, system warm-up, transient thermal dynamics, power management, mathematical modeling, model-based control, time-optimal control, feedback control.**

NOMENCLATURE

A, B, C, D	Coefficients of the linearized Hamiltonian
A_{Active}	Active area (m^2)
c	Specific heat (J/(kg K))
E	Thermodynamic potential (V)
f	System dynamics function
H	Hamiltonian
$\dot{H}$	Enthalpy flow rate (W)
h, $\tilde{h}$	Switching functions
I	Electric current (A)
J	Performance index (s)
j, k	Indices
m	Mass (kg)
$\dot{m}$	Mass flow rate (kg/s)
n_{Cells}	Number of fuel cells
P	Power (W)
Q	Battery capacity (C)
$\dot{Q}$	Heat flow rate (W)
R_i	Battery internal resistance (Ω)
s	Slack variable
SOC	Battery state of charge
T	Temperature (K)
t	Time (s)
Δt_c	Computation time (s)
Δt_s	Sample time (s)
u	Control vector
V	Voltage (V)
Vol	Volume (m^3)
v	External input vector
x	State vector

Greek Symbols

α, β, γ	Coefficients of the switching functions
η	Efficiency
λ	Costate vector
λ_{Air}	Air excess ratio
ν	Overvoltage (V)
Ω	Set of admissible control vectors
ρ	Mass density (kg/m^3)
τ	Time constant (s)

Subscripts and Superscripts

$*$	Optimal
0	Initial
Act	Activation
Amb	Ambient
Aux	Auxiliaries
av	Average
Bat	Battery
$Cell$	Fuel cell
$Cond$	Conduction
$Conv$	Convection
CS	Cooling system
Ct	Coolant
des	Desired value
$Evap$	Evaporation
Exs	Non-reacting part of the moist air flow
f	Final
Fan	Fan
HM	Humidification section
HT	Heater
HX	Heat exchanger
IF	Input filter
In	Inlet
$mAir$	Moist air
max	Maximum
$Mean$	Mean value

Manuscript received ??? ??, 200?; revised ??? ??, 200?. Manuscript received in final form ??? ??, 200?. Recommended by Associate Editor X. Yz.

E. A. Müller is with the Measurement and Control Laboratory, ETH Zurich, 8092 Zurich, Switzerland (e-mail: mueller@imrt.mavt.ethz.ch).

A. G. Stefanopoulou is with the Department of Mechanical Engineering, University of Michigan, Ann Arbor, MI 48109 USA (e-mail: annastef@umich.edu.

L. Guzzella is with the Measurement and Control Laboratory, ETH Zurich, 8092 Zurich, Switzerland (e-mail: guzzella@imrt.mavt.ethz.ch).

min	Minimum
mH_2	Moist hydrogen
nom	Nominal
oc	Open circuit
Ohm	Ohmic
Out	Outlet
PC	Power converter
PS	Power section
Rad	Radiation
$Reac$	Reaction
St	Stack
Sys	Fuel cell system

I. Introduction

FUEL cells are considered to be an alternative power source for automotive propulsion, electricity generation, and back-up power supplies. Their high specific power, low operating temperature characteristics, and ability to respond to rapid load changes make the polymer electrolyte membrane (PEM) fuel cells preferable for applications characterized by highly dynamic operating conditions. A particularly critical task, even for low-temperature fuel cell systems, is to overcome the transient power limitations during warm-up. The time needed to warm up the fuel cell system is of prominent importance. For example, customers of fuel cell vehicles will expect to start the vehicle and drive away almost immediately. A popular solution to this problem is the system hybridization. The basic idea of a hybrid setup is to combine the primary energy conversion device with an energy storage system, as for instance an electrochemical battery. In the case of cold start, the energy storage system can thus be used to guarantee the power output demanded throughout this phase and, preferably in combination with an auxiliary heating device, to accelerate the system warm-up.

A question emerging with the hybridization is the appropriate power management of the system's main components under transient temperature conditions. Many publications have discussed the importance of a well-designed power control, for example, see [1]–[3]. But the developed solutions exclude the warm-up issues and thus are designed for stationary temperature conditions only. The objective of the present study is to find an optimal power control strategy for the fuel cell stack and an auxiliary coolant heater during the temperature-transient phase after a cold start. As the system should attain its operating temperature as fast as possible, the elapsed system warm-up time is defined to be the measure of optimality. Preferably, the time-optimal control strategy developed should be implementable as a feedback controller to allow a real-time optimization of the power management.

In order to systematically develop a controller for the power management during the system warm-up, a control-oriented mathematical model of the system's transient behavior is required. Recently, several approaches of various levels of complexity have been proposed to predict the thermal characteristics of a fuel cell stack, for example, see [4]–[8]. In the present study a modified and extended version of the fuel cell stack model developed in [8] is employed. This model has to be extended with the other relevant components of the system, specifically, the coolant loop, the battery, the auxiliary heater, and a power converter.

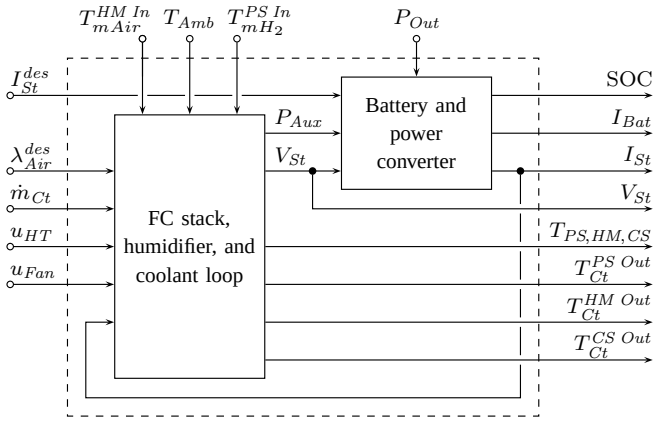

Fig. 1. Schematic of the input and output signals of the hybrid fuel cell power system model with power generation subsystem (left block) and power conversion and storage subsystem (right block).

In the first part of this paper the mathematical model of the hybrid fuel cell power system is described. The model is based on physical first principles and considers the relevant energy and mass flows. Sub-freezing conditions are not captured. The model assumes high-level supervisory power control and low-level control for each component. Where necessary, parameters of the model are identified experimentally, and the thermal part is validated against measurement data. At the end of the modeling section, a model with reduced order and complexity is proposed. This simpler model serves as a basis for the subsequent controller development. The derivation of the optimal warm-up controller is the focus of the second part. Therein, an optimal control problem is stated first. Applying Pontryagin's Minimum Principle, then, results in a set of necessary conditions for the optimality of a solution. On the basis of these conditions, a feedback control law for the optimal power management is derived. Implementation aspects for the real-time usage of the controller are also addressed. Moreover, the power controller is augmented with a coolant mass flow controller. In the third part of the paper a direct feedforward optimization environment is introduced. The direct feedforward optimization serves as a performance benchmark for the controller and it is also used to investigate the effects on the warm-up time of various system configurations (e. g. without auxiliary heater). In the last part, an optimally controlled system warm-up is analyzed in the simulation and the functionality of the controller developed is verified.

II. Model of the Hybrid Fuel Cell Power System

The model of the hybrid fuel cell power system consists of a power generation subsystem (power section, humidifier, and coolant loop) and a power conversion and storage subsystem (power converter and battery). A causality diagram of the model is shown in Fig. 1. The controllable inputs are the desired stack current, I_{St}^{des}, the desired air excess ratio, λ_{Air}^{des},

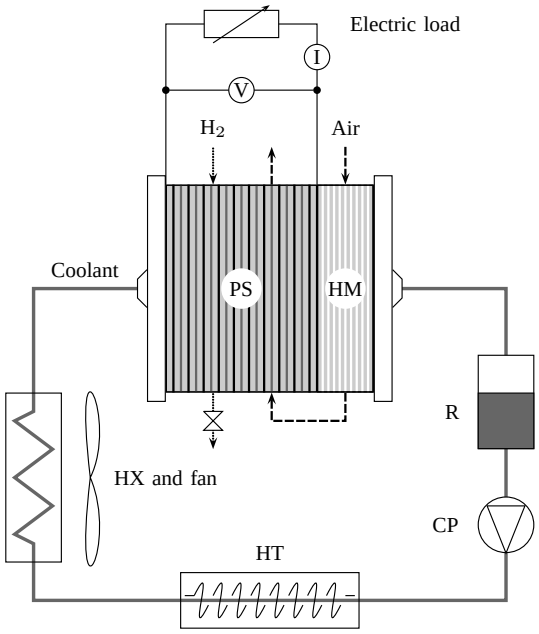

Fig. 2. Schematic of the fuel cell stack with integrated humidification section and of the coolant circuit layout. (PS: power section, HM: humidifier, R: reservoir, CP: coolant pump, HT: heater, HX: heat exchanger)

the coolant mass flow rate[1], $\dot{m}_{Ct}$, and the actuator signals of the heater and the fan, u_{HT} and u_{Fan}. The demanded system output power, P_{Out}, the ambient temperature, T_{Amb}, the air inlet temperature, $T_{mAir}^{HM\,In}$, and the hydrogen inlet temperature, $T_{mH_2}^{PS\,In}$, are uncontrollable but measurable input signals. The output signals of the system are the state of charge of the battery, SOC, the battery current, I_{Bat}, the stack current and voltage, I_{St} and V_{St}, the components' temperatures, T_{PS}, T_{HM}, and T_{CS}, and the coolant temperatures, $T_{Ct}^{PS\,Out}$, $T_{Ct}^{HM\,Out}$, and $T_{Ct}^{CS\,Out}$. The main component of the system is the fuel cell unit. In this project a 1.25 kW, 24-cell PEM fuel cell stack with an integrated membrane-type humidification section is considered. Detailed specifications of the fuel cell unit can be found in [8].

A. Modeling of the Power Generation Subsystem

A schematic overview of the power generation subsystem is depicted in Fig. 2. The power generation subsystem can be divided into two parts: the thermal part and the electric part.

1) Thermal Dynamics: The thermal dynamics module of the model predicts the temperatures of the main system components (fuel cell stack, humidifier, and cooling system) and the relevant coolant inlet and outlet temperatures. In order to capture the temperature dynamics of the system's main components, the first law of thermodynamics is applied to three separate control volumes, one for each component. For the power section, the energy balance yields the following differential equation:

$$\begin{aligned} m_{PS}\, c_{PS} \frac{dT_{PS}}{dt} = {} & \dot{H}_{Reac} - \dot{H}_{H_2O}^{Evap\,PS} + \Delta\dot{H}_{mAir\,Exs}^{PS} \\ & + \Delta\dot{H}_{Ct}^{PS} - \dot{Q}_{Cond}^{PS2HM} - \dot{Q}_{Conv}^{PS2Amb} \\ & - \dot{Q}_{Rad}^{PS2Amb} - P_{St}. \end{aligned} \tag{1}$$

This equation states that the rate of change of energy inside the control volume is equal to the reaction enthalpy rate (for liquid product water), minus the evaporation enthalpy flow rate of water inside the power section, plus the enthalpy flow rate difference of the moist excess air, plus the enthalpy flow rate difference of the coolant, minus the energy rate conducted to the adjacent humidification section, minus the rate of convective and radiative heat transfer to the environment, minus the electric power. Kinetic and potential energies of the mass streams are neglected, as they are small compared to the other contributions. Mass storage effects and the purging and leakage of hydrogen are not considered either. A detailed discussion of the relevant contributions to the power section energy balance can be found in [8]. For the calculation of the heat transfer to the coolant, $\Delta\dot{H}_{Ct}^{PS}$, and of the coolant temperature $T_{Ct}^{PS\,Out}$, a quasi-static, internal-flow, convective heat transfer with constant surface temperature is assumed. The air excess ratio is assumed to be perfectly controlled, hence, to follow exactly the desired value,

$$\lambda_{Air} = \lambda_{Air}^{des}. \tag{2}$$

Similarly to the energy balance (1), the energy balance for the humidification section yields

$$\begin{aligned} m_{HM}\, c_{HM} \frac{dT_{HM}}{dt} = {} & \Delta\dot{H}_{Ct}^{HM} - \dot{H}_{H_2O}^{Evap\,HM} + \Delta\dot{H}_{mAir}^{HM} \\ & + \dot{Q}_{Cond}^{PS2HM} - \dot{Q}_{Conv}^{HM2Amb} \\ & - \dot{Q}_{Rad}^{HM2Amb}. \end{aligned} \tag{3}$$

As shown in Fig. 2, the coolant circuit consists of a reservoir, the coolant pump, an electrical heater as heat source, and a heat exchanger with a fan to remove heat. In favor of a low-order model, the coolant system was lumped into one thermal mass of uniform temperature. The differential equation defining the cooling system temperature dynamics is given below.

$$\begin{aligned} m_{CS}\, c_{CS} \frac{dT_{CS}}{dt} = {} & \dot{m}_{Ct}\, c_{Ct} \left(T_{Ct}^{HM\,Out} - T_{CS}\right) \\ & + \dot{Q}_{HT} - \dot{Q}_{HX} \end{aligned} \tag{4}$$

The first term considers the enthalpy flows of the coolant entering and exiting the coolant loop, $\dot{Q}_{HT}$ is the thermal power supplied to the system by heating, and $\dot{Q}_{HX}$ represents the heat emitted at the heat exchanger. As the reservoir is not included explicitly in the model, the coolant refill has to be treated as a temperature disturbance. Due to the pipe volume a time lag has to be considered for the coolant temperature at the cooling system outlet (power section inlet). This time lag was approximated by a first-order delay,

$$\tau_{CS} \frac{dT_{Ct}^{CS\,Out}}{dt} = T_{CS} - T_{Ct}^{CS\,Out} \tag{5}$$

[1]On the test station the coolant flow rate is controlled through a manual valve. Therefore, instead of a coolant pump control signal, the coolant flow rate $\dot{m}_{Ct}$ is used as input signal.

with a time constant of

$$\tau_{CS} = \frac{\rho_{Ct}\, Vol_{CS}}{\dot{m}_{Ct}}. \tag{6}$$

2) Stack Voltage and Auxiliary Power: In order to predict the voltage output of the fuel cells, a quasi-static electrochemical model was implemented. This static voltage model predicts the cell voltage as a function of the relevant influencing variables. It considers the thermodynamic equilibrium potential, E, the activation overvoltage, ν_{Act}, and the ohmic overvoltage, ν_{Ohm},

$$V_{Cell} = E - \nu_{Act} - \nu_{Ohm}. \tag{7}$$

Mass concentration effects were not considered. The overvoltages were expressed as a combination of physical and empirical relationships. The stack voltage was then defined as the sum of the individual cell voltages, all of which were assumed to be equal.

$$V_{St} = n_{Cells}\, V_{Cell} \tag{8}$$

For the operation of a fuel cell system, auxiliary power is needed. The main power consumers of the fuel cell system investigated are the coolant pump, the air compressor, and the electrical heater. Since the power consumption of the first two is two to three orders of magnitude smaller than that of the electrical heater, it was neglected[2]. According to the correlations for the calculation of auxiliary component power given in [9], the power input of the coolant pump is estimated to stay below 20 W, and the power input of the air compressor is valued to be below 15 W. The electric power of the heat tape is assumed to be linearly dependent on the control signal u_{HT},

$$P_{Aux} = u_{HT}\frac{\dot{Q}_{HT}^{nom}}{\eta_{HT}}. \tag{9}$$

The value $\dot{Q}_{HT}^{nom}$ denotes the nominal thermal power of the heater and η_{HT} the heater efficiency, which are both assumed to be constant.

B. Modeling of the Power Conversion and Storage Subsystem

The existing power generation module was notionally augmented with a power conversion module (DC/DC power converter) and a power storage module (electrochemical battery) to form a hybrid power system. A schematic of the proposed electric layout is shown in Fig. 3. The battery and the electric load are connected in parallel to the main bus of the power converter.

1) Power Converter: The power converter module serves to determine the additionally required power from the battery or the surplus power, respectively, to provide the desired output power.

$$P_{Bat} = P_{Out} + P_{Aux} - \eta_{PC}\, I_{St}\, V_{St} \tag{10}$$

The model also allows for negative values of P_{Out}. Negative power demands may, for example, occur when considering regenerative braking in a hybrid vehicle application. A perfectly, low-level controlled system was assumed, implying that the actual stack current equals the desired stack current,

$$I_{St} = I_{St}^{des}. \tag{11}$$

In order to take into account the losses, a constant efficiency η_{PC} for the power conversion was presumed.

2) Battery: In the battery module the amount of energy buffered is calculated. The level variable of the stored energy is the state of charge of the battery, SOC.

$$Q_{Bat}\frac{d\mathrm{SOC}}{dt} = -I_{Bat} \tag{12}$$

The capacity of the battery is denoted by Q_{Bat}, and I_{Bat} is the battery current. As the battery voltage is a function of the battery current,

$$V_{Bat} = V_{oc}(\mathrm{SOC}) - R_i(\mathrm{SOC}, I_{Bat})\, I_{Bat} \tag{13}$$

the battery current can only be inferred recursively from the battery power,

$$I_{Bat} = \frac{P_{Bat}}{V_{Bat}(I_{Bat})}. \tag{14}$$

The value $V_{oc}(\mathrm{SOC})$ denotes the open circuit voltage of the battery, while $R_i(\mathrm{SOC}, I_{Bat})$ represents the internal resistance. The effect of any charge losses (coulomb efficiency) and the influence of temperature on the battery performance were not taken into consideration for this model.

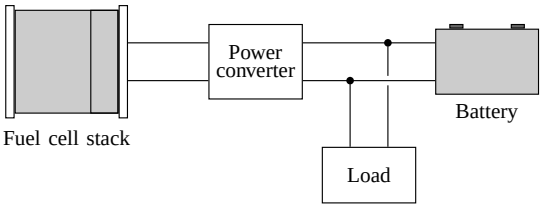

Fig. 3. Schematic of the electric system layout (hybrid system configuration) with the PEM fuel cell stack as energy source, a DC/DC power converter, and a battery as energy storage system.

C. Parametrization and Validation

As the model established is a control-oriented lumped-parameter model, and as the formulation of the model is mainly based on physical first principles, the model is relatively easy to parametrize. Where necessary and feasible, parameter values were identified with measurement data recorded on the test bench. Many parameters are geometrical parameters and can thus be determined in a straightforward fashion. Other parameters (e. g. heat transfer coefficients) were calculated based on known convection correlations, and a few parameter values were estimated. The parameters and characteristics of the battery were taken from a public database [10]. The battery was assumed to be a stack of ten modules, each of which consisting of six nickel metal hydride (NiMH) cells. Characteristic parameters of the model are summarized in Table I.

The power generation module was extensively validated against experimental data. In order to be able to estimate the dynamic quality of the model, the important input signals were

[2]Consider that the system investigated is a low-pressure system. The inclusion of a current-dependent air-compressor load is recommended when dealing with higher-pressure systems.

TABLE I
MAIN PARAMETERS OF THE HYBRID FUEL CELL POWER SYSTEM MODEL

Parameter	Symbol	Value
Rated fuel cell stack output power	P_{St}^{nom}	1.25 kW
Number of fuel cells	n_{Cells}	24
Cell active area	A_{Active}	296 cm^2
Nominal battery voltage	V_{Bat}^{nom}	72 V
Battery capacity (@ 6.5 A)	Q_{Bat}	6 Ah
Power converter efficiency	η_{PC}	0.95
Nominal thermal power of the HT	$\dot{Q}_{HT}^{nom}$	600 W
Efficiency of the HT	η_{HT}	0.8
Thermal capacity of the PS	$m_{PS}c_{PS}$	12 460 J/K
Thermal capacity of the HM	$m_{HM}c_{HM}$	5 460 J/K
Thermal capacity of the CS	$m_{CS}c_{CS}$	12 000 J/K
Volume of the CS	Vol_{CS}	0.75 L

varied during the experiments. Figure 4(a) shows the desired stack current, the coolant mass flow rate, and the heater and fan control signals. The desired air excess ratio was set to a constant value ($\lambda_{Air}^{des} = 2$). The predicted coolant temperatures at the cooling system outlet (power section inlet) and at the humidifier outlet, and the predicted stack voltage were compared with the corresponding measurement data to rate the quality of the model. As shown in Fig. 4(b), the prediction accuracy is excellent for the temperatures and adequate for the stack voltage. The good agreement between the experimental data and the simulation, even during heavy transients, reveals that the model derived captures the main static and dynamic properties of the system as expected.

D. Reduced-Order Model

The detailed, fifth-order model derived above was used to verify the functionality of the controller. However, it is too complex to be used for the development of an optimal controller. Therefore, a model of reduced complexity was established. This reduced-order model results from the following simplifications:

- Combination of the temperature variables T_{PS}, T_{HM}, T_{CS}, and $T_{Ct}^{CS\,Out}$ into one lumped state variable describing a mean system temperature.
- Modeling of the enthalpy rate of reaction independent of reactant and product temperatures.
- Neglect of the enthalpy flow difference of the excess air.
- Usage of average (constant) values for the battery open-circuit voltage and the battery internal resistance.

These simplifications yield a nonlinear, second order system of ordinary differential equations,

$$\frac{dT_{Sys}}{dt} = f_1(T_{Sys}, I_{St}^{des}, u_{HT}, u_{Fan}, \lambda_{Air}^{des}, T_{Amb}) \quad (15)$$

$$\frac{d\mathrm{SOC}}{dt} = f_2(T_{Sys}, I_{St}^{des}, u_{HT}, u_{Fan}, P_{Out}) \quad (16)$$

with state variables T_{Sys} (mean system temperature) and SOC (state of charge of the battery). The variables I_{St}^{des}, λ_{Air}^{des}, u_{HT}, and u_{Fan} are controllable input signals, whereas P_{Out} and T_{Amb} denote the uncontrollable external variables of the simplified system model.

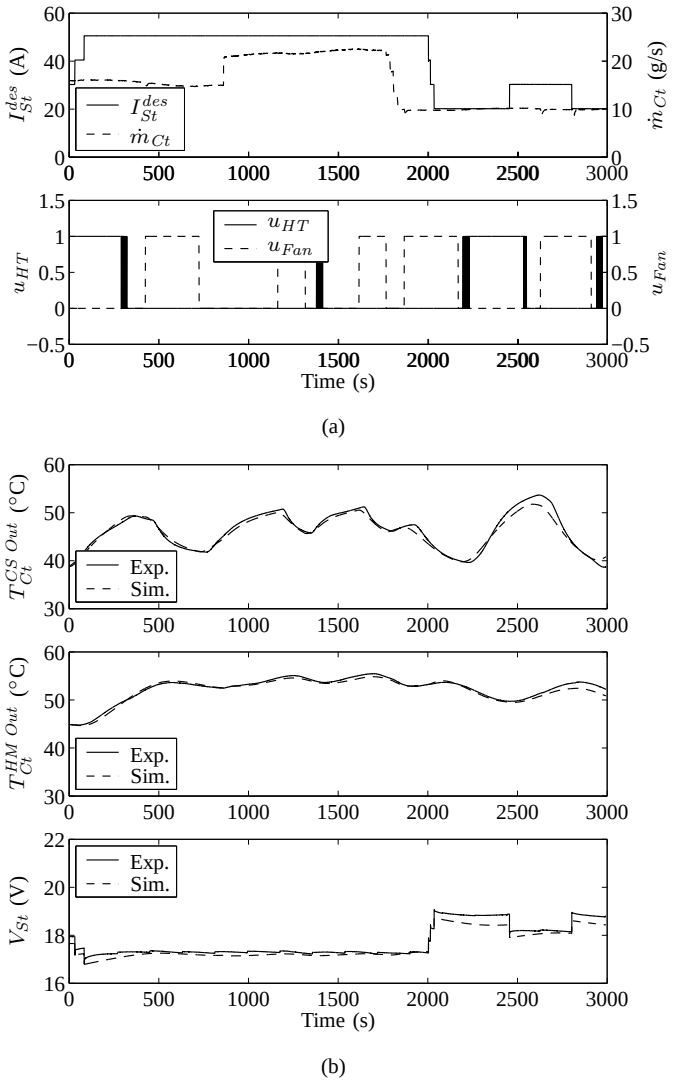

Fig. 4. Validation of the model: (a) input signals (the remaining inputs were assumed to be constant, $\lambda_{Air}^{des} \equiv 2$, $T_{Amb} \equiv 25°\mathrm{C}$, $T_{mAir}^{HM\,In} \equiv 20°\mathrm{C}$, $T_{mH_2}^{PS\,In} \equiv 40°\mathrm{C}$), (b) comparison between experiment and prediction of the coolant temperatures at the cooling system outlet and at the humidifier outlet, and of the stack voltage.

The dynamics of the mean system temperature, T_{Sys}, are calculated as

$$\begin{aligned} m_{Sys}\, c_{Sys} \frac{dT_{Sys}}{dt} &= \dot{H}_{Reac} - \dot{H}_{H_2O}^{Evap} \\ &\quad - \dot{Q}_{Conv}^{Sys2Amb} - \dot{Q}_{Rad}^{Sys2Amb} \\ &\quad + \dot{Q}_{HT} - \dot{Q}_{HX} - P_{St}. \end{aligned} \quad (17)$$

A slack variable, s, was introduced for the adjustment of the thermal capacity of the system,

$$m_{Sys}\, c_{Sys} = s \cdot \sum\nolimits_{k \in \{PS,HM,CS\}} m_k\, c_k. \quad (18)$$

The state of charge of the battery is still determined through (12) as a function of the battery current. But, by virtue of the constant open-circuit voltage and constant internal resistance assumption, (14) can be solved for the battery current,

$$I_{Bat} = \frac{V_{oc}^{av} - \sqrt{(V_{oc}^{av})^2 - 4\, R_i^{av} P_{Bat}}}{2\, R_i^{av}}. \quad (19)$$

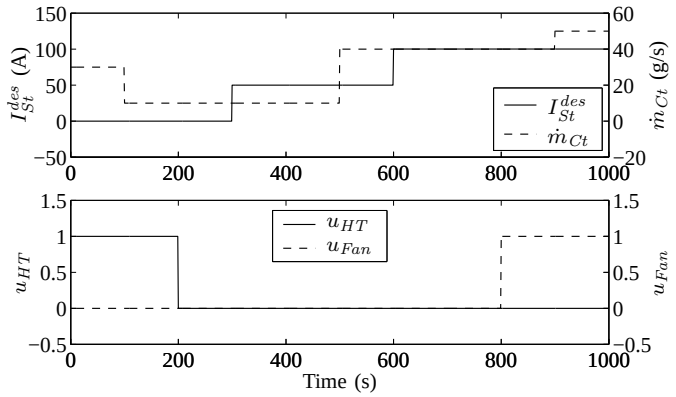

(a)

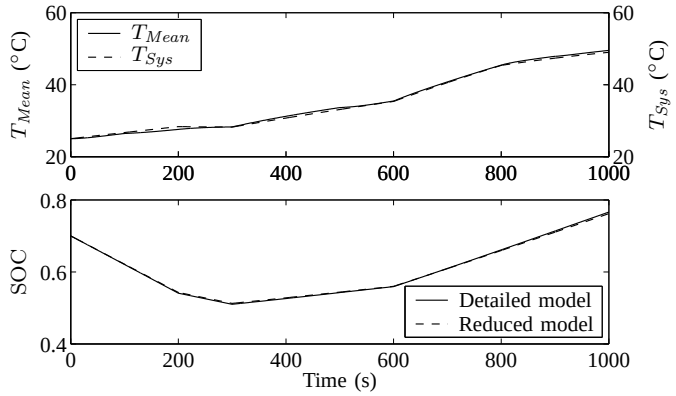

(b)

Fig. 5. Verification of the simplified system model: (a) input signals (the remaining inputs were set to be constant, $P_{Out} \equiv 500\,\mathrm{W}$, $\lambda_{Air}^{des} \equiv 2$, $T_{Amb} \equiv 25°\mathrm{C}$, $T_{mAir}^{HM\,In} \equiv 20°\mathrm{C}$, $T_{mH_2}^{PS\,In} \equiv 40°\mathrm{C}$, (b) comparison between the detailed model and the reduced-order model.

1) Verification: In Fig. 5(b) the simplified model is compared with the detailed model for a set of arbitrarily chosen input signals. A weighted mean temperature

$$T_{Mean} = \frac{\sum_{k\in\{PS,HM,CS\}} m_k\, c_k\, T_{Ct}^{k\,Out}}{\sum_{k\in\{PS,HM,CS\}} m_k\, c_k} \tag{20}$$

was defined as a reference signal for the temperature T_{Sys}. The slack variable was set to $s = 1.15$. Apparently, the reduced-order model can be applied to predict accurately the mean temperature of the system and the state of charge of the battery, as the results of Fig. 5(b) demonstrate. This validates the simplifications introduced. Additionally, the results prove the fact that the coolant mass flow rate has no influence on the mean temperature (but only on the spreading of the component temperatures).

III. Development of the Optimal Supervisory Controller

A feedback controller was developed based on the simplified model equations (15) and (16) for the optimal supervisory control during the transient warm-up phase. The warm-up phase of the hybrid fuel cell system is defined as the time period before the mean system temperature reaches a predefined operating temperature value T^f.

$$\text{Warm-up completed} \;\Leftrightarrow\; T_{Sys}(t_f) = T^f \tag{21}$$

The controller operates the system to heat up within minimal time while taking into account energy and temperature constraints. The energy constraint enables the charge-sustaining operation and predefines the value of the battery's terminal state of charge, SOC^f. The temperature constraint ensures that the spacial temperature gradient of the system is bounded.

The controller is divided into two sub-controllers: an optimal warm-up power controller and a warm-up cooling system controller. For the optimal warm-up power controller two control variables are considered, namely, the desired stack current, I_{St}^{des}, and the heater control signal, u_{HT}. As the current density of the fuel cells is limited, the allowed stack current is bounded in magnitude,

$$I_{St}^{des} \le I_{St}^{max}. \tag{22}$$

It is possible to consider a temperature dependency in the current density restriction to take into account the variability of the membrane performance. The output power, P_{Out}, the ambient temperature, T_{Amb}, and the desired air excess ratio, λ_{Air}^{des}, were treated as external variables, since they are not controllable or are assumed to be controlled on a different level of the control hierarchy. The coolant mass flow rate, $\dot{m}_{Ct}$, which was shown to have no influence on the systems's mean temperature, is regulated by the cooling system controller. For obvious reasons, the heat exchanger fan is assumed to be off during the entire warm-up period,

$$u_{Fan} \equiv 0. \tag{23}$$

A. Statement of the Optimal Warm-up Control Problem

The problem of minimizing the system warm-up time constitutes a minimum-time optimal control problem. In order to simplify the notation during the subsequent optimization part, the following substitutions are introduced:

$$x = [x_1, x_2]^T = [T_{Sys}, \mathrm{SOC}]^T \tag{24}$$

$$u = [u_1, u_2]^T = [\frac{I_{St}^{des}}{I_{St}^{max}}, u_{HT}]^T \tag{25}$$

$$v = [v_1, v_2, v_3]^T = [P_{Out}, T_{Amb}, \lambda_{Air}^{des}]^T. \tag{26}$$

The optimal control problem is stated as follows:
Let x_0 be a given initial state of the system. Find an optimal control vector $u^* : [t_0, t_f] \to \Omega \subseteq \mathbb{R}^2$, such that the following conditions are met:

$$x^*(t_0) = x^0 \tag{27}$$

$$\dot{x}^*(t) = f(x^*(t), u^*(t), v), \qquad \text{for all } t \in [t_0, t_f] \tag{28}$$

$$x^*(t_f) = x^f \tag{29}$$

and the performance index

$$J(u) = \int_{t_0}^{t_f} 1\, dt = t_f - t_0, \qquad t_f \text{ free} \tag{30}$$

is minimized.

The condition (29) constrains the components of the state vector at terminal time to have the prescribed values,

$$x^f = [T^f, \mathrm{SOC}^f]. \tag{31}$$

The components of the control vector are constrained in magnitude by the relation

$$u_1(t), u_2(t) \in [0, 1]. \tag{32}$$

The uncontrollable input signals v appear as disturbances. As they are generally not known in advance, they are assumed to be constant for the formulation of the optimal control problem.

This idea will become clearer later on. The Hamiltonian $H : \mathbb{R}^2 \times \Omega \times \mathbb{R}^2 \to \mathbb{R}$ associated with this (time-invariant) optimal control problem is given by

$$H(x(t), u(t), \lambda(t)) = 1 + \lambda^T(t)\, f(x(t), u(t), v) \tag{33}$$

where $\lambda(t)$ denotes the costate vector.

B. Necessary Conditions for the Optimality of a Solution

If $u^* : [t_0, t_f^*] \to \Omega$ is an optimal control vector, the following necessary conditions hold [11]:

$$\dot{x}^*(t) = \nabla_\lambda H(x^*(t), u^*(t), \lambda^*(t)) \tag{34}$$

$$x^*(t_0) = x^0 \tag{35}$$

$$x^*(t_f^*) = x^f \tag{36}$$

$$\dot{\lambda}^*(t) = -\nabla_x H(x^*(t), u^*(t), \lambda^*(t)) \tag{37}$$

$$H(x^*(t), u^*(t), \lambda^*(t)) \equiv 0 \tag{38}$$

$$H(x^*(t), u^*(t), \lambda^*(t)) \le H(x^*(t), u, \lambda^*(t)), \quad \text{for all } u \in \Omega,\ t \in [t_0, t_f^*]. \tag{39}$$

Below, the explicit statement of the time dependency as well as the indication of v are omitted for the sake of brevity.

C. Derivation of the Optimal Feedback Control Law

For the solution of the optimal control problem stated above it is assumed that the optimal control problem is normal[3]. Hence, the derivation of the feedback control law consists of two consecutive steps. First, the H-minimal control is derived from (39). This preliminary control law relates the control signal u to the state x and to the costate λ. In a second step, two equations are deduced from the necessary conditions (34)–(38) to eliminate the costate λ.

1) H-minimal Control: In order to avoid the need for any second-order conditions for the derivation of the H-minimal control, the Hamiltonian is linearized in the control vector, yielding

$$\begin{aligned} H(x, u, \lambda) \approx 1 &+ \lambda_1\, A(x_1) + \lambda_2\, C(x_1) \\ &+ [\lambda_1\, B_1(x_1) + \lambda_2\, D_1(x_1)]\, u_1 \\ &+ [\lambda_1\, B_2 + \lambda_2\, D_2]\, u_2. \end{aligned} \tag{40}$$

Physically interpreted, this step corresponds to linear approximations of the equation for the battery current, $I_{Bat} = I_{Bat}(P_{Bat})$, and of the equation for the stack power, $P_{St} = P_{St}(I_{St})$. At this point, usually, substitutions for the coefficients of the control components are introduced (switching functions).

$$h_1(x_1, \lambda_1, \lambda_2) = \lambda_1\, B_1(x_1) + \lambda_2\, D_1(x_1) \tag{41}$$

$$h_2(\lambda_1, \lambda_2) = \lambda_1\, B_2 + \lambda_2\, D_2 \tag{42}$$

The H-minimal control thus can be expressed as

$$u_j^* = \begin{cases} 1 & \text{if } h_j^* < 0 \\ 0 & \text{if } h_j^* > 0 \\ \text{indeterminate} & \text{if } h_j^* = 0 \end{cases}, \qquad \text{for } j = 1, 2. \tag{43}$$

In a normal optimal control problem, by definition, the functions h_j^* can be zero only at isolated instants of time. Hence, the time-optimal controls consist of piecewise constant functions (of value 0 or 1) with simple jumps.

2) Elimination of the Costate Vector: Under the restriction

$$\dot{x}_1^* \approx A(x_1^*) + B_1(x_1^*)\, u_1^* + B_2\, u_2^* \neq 0 \tag{44}$$

the necessary condition (38) can be transformed into an equation for the costate λ_1^*,

$$\lambda_1^* = -\frac{1 + \lambda_2^* \left[C(x_1^*) + D_1(x_1^*)\, u_1^* + D_2\, u_2^*\right]}{A(x_1^*) + B_1(x_1^*)\, u_1^* + B_2\, u_2^*}. \tag{45}$$

After the multiplication with the denominator of (45) the substitution of (45) into the switching functions (41) and (42) yields the modified switching functions $\tilde{h}_1$ and $\tilde{h}_2$,

$$\begin{aligned} \tilde{h}_1(x_1, \lambda_2, u_2) = {} & \lambda_2\, D_1(x_1)\, A(x_1) \\ & - \lambda_2\, B_1(x_1)\, C(x_1) - B_1(x_1) \\ & + \lambda_2 \left[D_1(x_1)\, B_2 - B_1(x_1)\, D_2\right] u_2 \end{aligned} \tag{46}$$

$$= \alpha(x_1, \lambda_2) + \gamma(x_1, \lambda_2)\, u_2 \tag{47}$$

$$\begin{aligned} \tilde{h}_2(x_1, \lambda_2, u_1) = {} & \lambda_2\, D_2\, A(x_1) - \lambda_2\, B_2\, C(x_1) - B_2 \\ & - \lambda_2 \left[D_1(x_1)\, B_2 - B_1(x_1)\, D_2\right] u_1 \end{aligned} \tag{48}$$

$$= \beta(x_1, \lambda_2) - \gamma(x_1, \lambda_2)\, u_1. \tag{49}$$

In order to prevent sign changes in the conditions of the H-minimizing control (43), the following restriction is required:

$$\dot{x}_1^* \approx A(x_1^*) + B_1(x_1^*)\, u_1^* + B_2\, u_2^* > 0. \tag{50}$$

Due to the fact that the signs of the linear parts of the affine switching functions (47) and (49) are different, the implicit relations $u_1^* = u_1(x_1^*, \lambda_2^*, u_2^*)$ and $u_2^* = u_2(x_1^*, \lambda_2^*, u_1^*)$ following from (43), (47), and (49) can uniquely be solved to determine u_1^* and u_2^*, as can be shown.

$$u_1^* = u_1(x_1^*, \lambda_2^*) \tag{51}$$

$$u_2^* = u_2(x_1^*, \lambda_2^*) \tag{52}$$

From the necessary condition (37) it is deduced that the costate λ_2 has to be constant on an optimal trajectory, as x_2 does not emerge in the Hamiltonian (33),

$$\dot{\lambda}_2^* = 0 \ \Rightarrow\ \lambda_2^* = \text{constant}. \tag{53}$$

[3]The optimal solution contains no singular arc.

By integrating the system dynamics (34) and considering the boundary constraints (35) and (36), the following necessary conditions for the optimal trajectory are obtained:

$$\int_{t_0}^{t_f} f_1(x_1^*, u_1^*, u_2^*)\, dt = x_1^f - x_1^0 \tag{54}$$

$$\int_{t_0}^{t_f} f_2(x_1^*, u_1^*, u_2^*)\, dt = x_2^f - x_2^0. \tag{55}$$

These conditions can be transformed to

$$\int_{x_1^0}^{x_1^f} \frac{f_2(x_1, u_1(x_1, \lambda_2^*), u_2(x_1, \lambda_2^*))}{f_1(x_1, u_1(x_1, \lambda_2^*), u_2(x_1, \lambda_2^*))}\, dx_1 + x_2^0 - x_2^f = 0 \tag{56}$$

by substituting

$$dt = \frac{dx_1}{f_1(x_1, u_1, u_2)} \tag{57}$$

into (55), adapting the integration limits, and replacing u_1^* and u_2^* with the control laws (51) and (52). The integral equation (56) defines implicitly the optimal (constant) value of the second costate component λ_2^*,

$$\lambda_2^* = \lambda_2(x_1^0, x_2^0, x_1^f, x_2^f). \tag{58}$$

The substitution (57) holds for $f_1 \neq 0$. Substituting (58) into (51) and (52) eventually yields the desired feedback control law,

$$u_1^* = u_1(x_1, x_1^0, x_2^0, x_1^f, x_2^f) \tag{59}$$

$$u_2^* = u_2(x_1, x_1^0, x_2^0, x_1^f, x_2^f). \tag{60}$$

D. Remarks Concerning the Existence of Optimal and Extremal Controls

In general, the questions about the existence of optimal controls from any initial state to any target set are extremely difficult to answer and the proper treatment of singular solutions is very complex. Therefore, motivated from an engineering point of view, the optimal control law derived was extended with a heuristic control law. The heuristic control law comes into operation if no zero λ_2^* of the integral equation (56) is found under the restriction $f_1(x_1, u_1(x_1, \lambda_2^*), u_2(x_1, \lambda_2^*)) > 0,\ \forall\ x_1 \in [x_1^0, x_1^f]$. The question about the existence of only locally optimal solutions is transferred to the question about the number of zeros of the integral equation (56). The optimal control law can potentially yield a locally optimal solution.

E. Optimal Warm-up Power Controller Implementation

While the previous section shows the procedure to derive the optimal control signals, this sections details how the equations derived are implemented in a feedback controller which optimizes the operation of the system on-line. The controller is assumed to work with a sample time of Δt_s and to require a computation time of Δt_c. The predefined terminal temperature, T^f, the predefined state of charge of the battery, SOC^f, and a filter time constant, τ_{IF}, are the only free parameters of the controller. The controller works according to the iteration scheme outlined below.

1) Determine the low-pass-filtered signal of the power demand at time t_j, where $t_{j-1} = t_j - \Delta t_s$,

$$P_{Out}^{IF}(t_j) = e^{-\frac{\Delta t_s}{\tau_{IF}}}\, P_{Out}^{IF}(t_{j-1}) + \left(1 - e^{-\frac{\Delta t_s}{\tau_{IF}}}\right) P_{Out}(t_j) \tag{61}$$

and assign the input signals,

$x_1^0 = T_{Mean}(t_j)$ (feedback signal)
$x_2^0 = \mathrm{SOC}(t_j)$ (feedback signal)
$v_1 = P_{Out}^{IF}(t_j)$ (low-pass-filtered external signal)
$v_2 = T_{Amb}(t_j)$ (external signal)
$v_3 = \lambda_{Air}^{des}(t_j)$. (external signal)

2) Calculate (iteratively) a constant λ_2,

$$\lambda_2 = \lambda_2(x_1^0, x_2^0, x_1^f, x_2^f, v_1, v_2, v_3)$$

subject to

$$f_1(x_1, u_1(x_1, \lambda_2), u_2(x_1, \lambda_2)) > 0,\ \forall\ x_1 \in [x_1^0, x_1^f]$$

with

$x_1^f = T^f$ (desired terminal temperature)
$x_2^f = \mathrm{SOC}^f$. (desired terminal state of charge)

3) If an admissible value for λ_2 is found, calculate the optimal control signals,

$$u_1 = u_1(x_1^0, \lambda_2, v_1, v_2, v_3)$$
$$u_2 = u_2(x_1^0, \lambda_2, v_1, v_2, v_3).$$

Else (if no admissible value for λ_2 is found), determine heuristically motivated control signals,

$$[u_1, u_2]^T = \begin{cases} [0,0]^T & \text{if } x_2^0 \geq x_2^f \\ [1,0]^T & \text{if } x_2^0 < x_2^f \end{cases}.$$

4) Assign the output signals,

$I_{St}^{des}(t) = u_1 \cdot I_{St}^{max}$ (stack control signal)
$u_{HT}(t) = u_2$ (heater control signal)

for $t_j + \Delta t_c \leq t < t_{j+1} + \Delta t_c$, and $t_{j+1} = t_j + \Delta t_s$.

In the following, the different steps of the control algorithm are elaborated.

1) Input Signals: The controller features two feedback signals: the mean system temperature, T_{Mean}, and the estimated state of charge of the battery, SOC. The mean system temperature can be obtained from measurements of the coolant temperatures, according to (20), whereas the state of charge has to be inferred through estimation. The details on the process of estimating the state of charge of a battery are outside the scope of this article and, therefore, not considered here. For reference, see for example [12].

The optimal feedback control law (model predictive control) determines the control signals under the assumption that the external variables (26) are constant, whereas in practice, these signals vary with time. Therefore, aside from the state feedback signals, a controller suitable for practical implementation has to possess the additional input signals P_{Out}, T_{Amb}, and

λ_{Air}^{des}. Repeatedly applying the control scheme with varying external signals thus means to repeatedly optimize the system, assuming the future external conditions to be constant for the rest of the warm-up. Unlike the ambient temperature, T_{Amb}, and the air excess ratio, λ_{Air}^{des}, which do not vary much in general, the demanded output power, P_{Out}, can fluctuate rapidly. In order to improve the prediction, therefore, the power signal is low-pass filtered at the input of the controller. Hence, the estimation of the averaged load conditions ahead is inferred from the past power demand. The time constant of the filter, τ_{IF}, is a free parameter of the controller.

2) Iterative Calculation of λ_2: As the conditional equation (56) for the costate component λ_2 is an integral equation, the zero finding is performed iteratively. The iteration terminates if a given function tolerance is met and aborts if a maximum number of iterations is reached or if the constraint for f_1 is violated. If the algorithm fails in finding a zero, the controller switches to the heuristic control law. The optimal value of the costate component λ_2 would be constant for an entire warm-up if the real system behaved exactly like the model. In practice, obviously, this value has to be adapted while the warm-up proceeds. As an initial guess, the value of the previous iteration is taken.

3) Calculation of the Control Signals: The optimal control signals are defined by the switching function coefficients $\alpha = \alpha(x_1^0, \lambda_2, v_1, v_2, v_3)$, $\beta = \beta(x_1^0, \lambda_2, v_1, v_2)$, and $\gamma = \gamma(x_1^0, \lambda_2, v_1, v_3)$. Alternatively, if no value for λ_2 is available, the controls are defined by heuristic rules. The heuristic extension of the control law runs the fuel cells with maximum power and switches the heater off if the current state of charge of the battery is below the desired terminal state of charge. If the current state of charge is above the desired terminal state of charge, both the fuel cell stack and the electrical heater are turned off.

4) Output Signals: The optimal control signals are computed every time step for the new initial conditions x^0 and external variables v, and are applied during the time interval from $t_j + \Delta t_c$ to $t_{j+1} + \Delta t_c$.

F. Coolant Flow Controller

The function of the coolant flow controller is to maintain a uniform temperature distribution within the fuel cell stack to guarantee high conversion efficiency of the fuel cells on the one hand, and to avoid damage to the stack through mechanical stress or hot spots, on the other hand. Thus, the coolant flow control maintains a minimum flow rate for low power conditions,

$$\dot{m}_{Ct} \geq \dot{m}_{Ct}^{min} \tag{62}$$

and ensures that a maximum temperature difference over the power section is not exceeded during high power demands,

$$T_{Ct}^{PS\ Out} - T_{Ct}^{PS\ In} \leq \Delta T_{PS}^{max}. \tag{63}$$

The temperature difference of the coolant over the power section, ΔT_{PS}, is the input signal and the coolant mass flow rate, $\dot{m}_{Ct}$, is the output signals of the controller. The coolant flow controller was realized as a PI controller with an anti-reset windup addition.

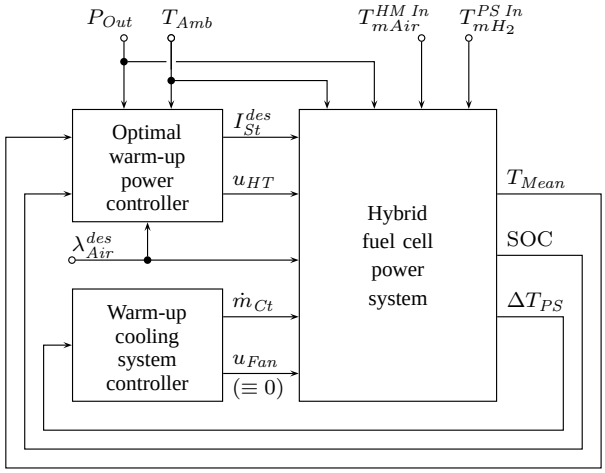

Fig. 6. Schematic of the control system structure for an optimally controlled system warm-up with the optimal warm-up power controller and the warm-up cooling system controller.

G. Control System Structure

A schematic of the control system structure for an optimally controlled system warm-up is depicted in Fig. 6. The control system features two controllers: the optimal warm-up power controller and the warm-up cooling system controller. The optimal warm-up power controller computes the optimal stack current and the optimal heater control signal during the warm-up period ($T_{Mean} \leq T^f$). The cooling system is controlled separately. During the warm-up, the fan is off, and the coolant flow controller ensures that the coolant does not exceed a maximum temperature difference over the fuel cell stack. Upon completion of the warm-up, the fan has to be operated to maintain the desired system temperature.

IV. Direct Feedforward Optimization

Besides the development of a feedback controller, the optimal control problem considered was also solved by a direct trajectory optimization method in a feedforward manner. Therefore, the problem of minimizing the warm-up time was implemented in GESOP[4], a software system for numerical trajectory optimization of dynamic systems [13]. In order to discretize the optimal control problem and to transcribe it into a parametrized, finite-dimensional optimization problem, the multiple shooting method PROMIS[5] was used. The standard nonlinear program (NLP) solver SLLSQP[6] was then applied to solve the resulting algebraic optimization problems for various operating conditions and parameter values. The control signals were approximated by piecewise linear functions. For the problem at hand, the number of corresponding subintervals was set to 12, resulting in 11 internal nodes whose positions in turn are subject to optimization. Additional control refinement points were defined where necessary.

The direct optimization method was applied for two purposes. It was first used to quantify the influence on the warm-up time of the hybridization and the extension of the fuel

[4]**G**raphical **E**nvironment for **S**imulation and **Op**timization
[5]**P**arametrized T**r**ajectory **O**ptimization by Direct **M**ult**i**ple **S**hooting
[6]**S**equential **L**inear **L**east **S**quares **Q**uadratic **P**rogramming

TABLE II
DEFINITION OF CONTROLLER PARAMETERS AND NOMINAL OPERATING CONDITIONS

Parameter / signal	Symbol	Value
Terminal temperature	T^f	50°C
Terminal state of charge	SOC^f	0.7
Input filter time constant	τ_{IF}	60 s
Power controller sample time	Δt_s	3 s
Power controller computation time	Δt_c	0.05 s
Minimum coolant flow rate	$\dot{m}_{Ct}^{min}$	10 g/s
Maximum temperature gap over the PS	ΔT_{PS}^{max}	10°C
Starting temperatures (PS, HM, CS)	$T_\bullet(0)$	25°C
Initial state of charge	$\mathrm{SOC}(0)$	0.7
Power demand	P_{Out}	500 W
Ambient temperature	T_{Amb}	25°C
Desired air excess ratio	λ_{Air}^{des}	2
Air inlet temperature	$T_{mAir}^{HM\,In}$	20°C
Hydrogen inlet temperature	$T_{mH_2}^{PS\,In}$	40°C

TABLE III
OPTIMAL SYSTEM PERFORMANCE FOR VARIOUS SYSTEM CONFIGURATIONS UNDER NOMINAL OPERATING CONDITIONS

Battery	Heater	$I_{St}^{des}(t)$	$u_{HT}(t)$	J^* (s)	$\delta J^{*\dagger}$ (%)
No	No	$f(P_{Out})$	-	3 487.0	0
Yes	No	optimized	-	971.4	-72
No	Yes	$f(P_{Out}, u_{HT})$	optimized	408.1	-88
Yes	Yes	optimized	optimized	311.8	-91

† Relative performance difference with respect to the configuration without battery nor heater: $\delta J^* = (J^* - J^*|_{\mathrm{No\,Bat,\,No\,HT}})/J^*|_{\mathrm{No\,Bat,\,No\,HT}}$.

cell system with an auxiliary heater. Second, the feedforward optimized solutions were used as performance benchmarks for the feedback-controlled system.

V. RESULTS AND DISCUSSION

As a basis for the evaluation which is the subject of the subsequent sections, nominal operating conditions were defined and parameter values for the controllers were proposed. These figures are given in Table II.

A. Investigation of Alternative System Configurations

In addition to the system configuration introduced in the modeling section, three alternative system configurations are proposed: a system without battery nor heater, a hybrid system without heater, and a system without energy storage unit but with an auxiliary heater. In Table III these configurations are compared with respect to their optimal performance values, J^*, i. e. their minimal warm-up times. The operating conditions were chosen according to the definitions of Table II. For simplification, the cooling system controller was disabled and the coolant mass flow signal was set to a constant ($\dot{m}_{Ct} = 35$ g/s). For configurations without an energy storage unit, the stack current, I_{St}^{des}, follows directly from the total power demand, as the number of degrees of freedom is diminished by one.

TABLE IV
BENCHMARK RESULTS FOR THE CONTROLLER UNDER VARIOUS OPERATING CONDITIONS

Operating conditions	$J^{*\dagger}$ (s)	$\delta J^{\ddagger}$ (%)
Nominal (Table II)	311.8	0.3
Nominal (Table II) but $P_{Out} = 250$ W	370.0	1.4
Nominal (Table II) but $P_{Out} = 750$ W	270.5	0.7
Nominal (Table II) but $P_{Out} = 1200$ W	251.0	2.4
Nominal (Table II) but $\lambda_{Air}^{des} = 3$	335.8	0.1
Nominal (Table II) but $T_{Amb} = T_\bullet(0) = 15$°C	432.7	0.0
Nominal (Table II) but $\mathrm{SOC}(0) = 0.65$	260.6	0.4
Nominal (Table II) but $\mathrm{SOC}(0) = 0.8$	415.0	1.7

† Minimum warm-up time from the direct feedforward optimization.
‡ Relative performance loss of the controller: $\delta J = (J|_{\mathrm{Controlled}} - J^*)/J^*$.

The configuration with no battery nor heater serves as a basis for the comparison. For nominal operating conditions it takes this system almost one hour (3 487 s) to reach the operating temperature of 50°C. The hybridization can reduce the elapsed warm-up time by 72% to 971 s, provided that optimal power management is applied. Another 68% reduction to 312 s can be gained by adding an (optimally controlled) auxiliary heater. Hence, the combination of hybridization and auxiliary heating yields a warm-up time of below one tenth (9%) of the reference value. A system configuration with auxiliary heater but without battery has a warm-up period reduced by 88% compared to the reference configuration.

The improvement achieved with the hybridization is explained by the additional degree of freedom. As a direct consequence of the possibility to store energy, the fuel cell stack can be operated over a shorter period of time with higher (maximum) power. This, in turn, results in reduced heat losses to the environment. Similarly, the auxiliary heater adds a degree of freedom to the system, too, but acts on the warm-up twofold. Primarily, and analogously to the battery, it permits the fuel cell stack to be operated on a higher power level and, secondarily, it delivers energy to the system directly in terms of heat.

B. Benchmark Tests for the Optimal Controller

During the development of the optimal warm-up controller, certain approximations or assumptions had to be made at some points (e. g. model reduction, linearization of the Hamiltonian). In order to quantify their impact and that of the discrete operation of the controller on the performance of the system, the performance values of the feedback controlled solutions were compared with the optimal warm-up times, J^*, emerging from the direct feedforward optimization. The parameters of the controller were set to their nominal values (Table II) and the coolant controller was disabled (constant coolant mass flow rate of $\dot{m}_{Ct} = 35$ g/s). In Table IV the results of the benchmark analysis are shown for various operating conditions. For the situations investigated, the relative performance loss of the controller with respect to the feedforward-optimized solution, δJ, is below 2.4%. This result indicates that the assumptions and approximations made are feasible and thus

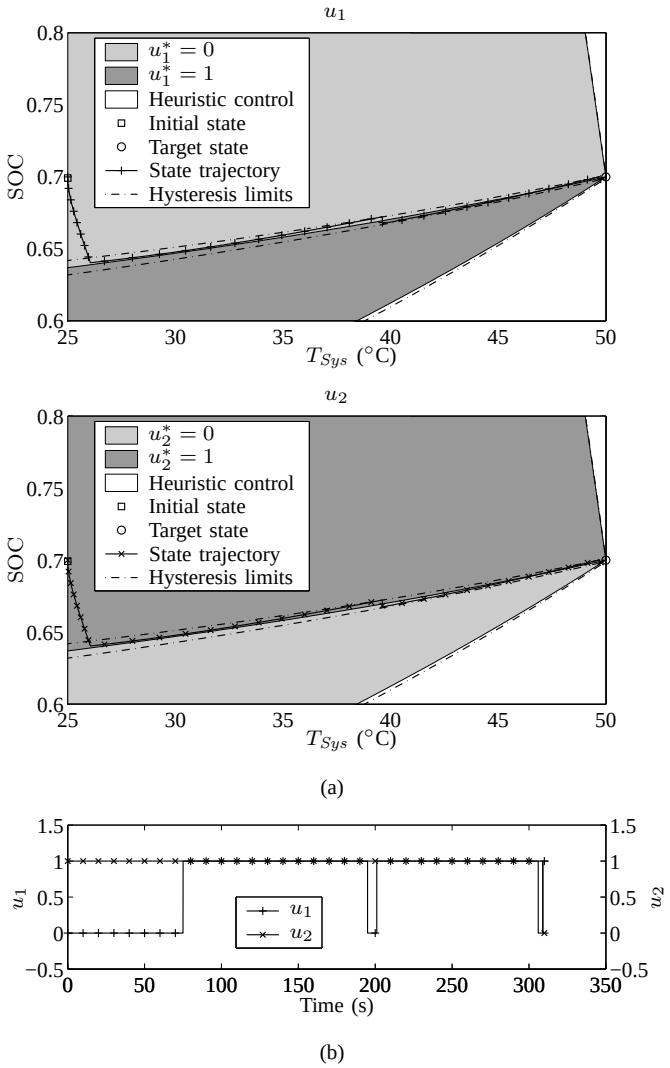

Fig. 7. Illustration of the controller operation for nominal operating conditions and controller parameters: (a) state plane illustration of the control law and of the state trajectory of the optimally controlled system, (b) corresponding control signals.

legitimates the methods applied for the controller development and implementation.

C. Illustration in the State Plane

In Figure 7(a) the switch curves of the optimal control are illustrated in the state plane. For each control variable, the switch curves divide the state space into regions over which the corresponding control variable is constant (0 or 1). The shapes of these switch curves, which are functions of the model and of the controller parameters (target state vector) as well as of the operating conditions, determine the characteristics of the controller. The operation of the controller is additionally affected by the value of the function tolerance used to terminate the iterative calculation of λ_2. The termination tolerance results in hystereses in the switching logic. In Fig. 7(a), these hystereses are indicated by dash-dotted lines along the switch curves. The blank regions in Fig. 7(a) represent the set of input state vectors for which the control law yields no solution. Inside these areas, the controls are determined by the heuristic rule: if $\mathrm{SOC} \geq \mathrm{SOC}^f$, both control signals are set to zero, $u_1 = u_2 = 0$, and if $\mathrm{SOC} < \mathrm{SOC}^f$, the fuel cell stack is turned on, and the heater off, $u_1 = 1$ and $u_2 = 0$, respectively. Inside the upper region ($\mathrm{SOC} \geq \mathrm{SOC}^f$), the heuristic rule causes the system to enter into the control region with $u_1^* = 0$ and $u_2^* = 1$, whereas inside the lower region, the heuristic controls force the system trajectory to proceed parallel to the region boundary. Trajectories inside the lower heuristic region can not reach the target state.

The operation of the controller for nominal operating conditions and controller parameters (Table II), with a coolant mass flow rate of $\dot{m}_{Ct} = 35\,\mathrm{g/s}$ is illustrated in Fig. 7(a) and 7(b). Figure 7(a) shows the state trajectory of the optimally controlled system in the state plane. In Fig. 7(b), the corresponding control signals are shown against time. The state trajectory of the controlled system starts at the initial state ($T_{Sys}(0) = 25°\mathrm{C}$, $\mathrm{SOC}(0) = 0.7$) and reaches a switch curve for u_1 after approximately 75 s. At that moment the stack control signal changes from $u_1 = 0$ to $u_1 = 1$. The state trajectory then follows the switch curve for about 120 s. Due to model uncertainties the state trajectory crosses the hysteresis limit at an elapsed time of approximately 195 s. This causes the controller to turn off the stack ($u_1 = 0$). As a consequence, the state trajectory crosses the hysteresis limit in the opposite direction. Soon after, when the trajectory exits the hysteresis area (at the other boundary), the stack is turned on again ($u_1 = 1$). A similar control action can be observed just before the end of the warm-up, where a final control action is necessary to reach the target state. During almost the entire warm-up phase the heater is on ($u_2 = 1$).

D. Optimally Controlled System Warm-up Under Variable Operating Conditions

A warm-up under variable power demands is used to demonstrate the full functionality of the optimal feedback control system developed. For this functionality analysis, the power signal of Fig. 8(a) is used. Apart from the power demand, the nominal operating values of Table II are applied to the system. Besides the power demand at the input of the system, Fig. 8(a) also shows the low-pass-filtered signal P_{Out}^{IF}. It can be shown that the choice of the time constant τ_{IF} of the input filter (61) is not critical, i. e. the elapsed warm-up time is only slightly affected by τ_{IF} over a broad range of values. The time constant was set to $\tau_{IF} = 60\,\mathrm{s}$. The first and the second subplots of Fig. 8(b) show the output signals of the optimal warm-up power controller. For the desired stack current, I_{St}^{des}, a temperature-dependent upper limit, $I_{St}^{max} = I_{St}^{max}(T_{Mean})$, was defined to take into account cold-start transient power limitations (indicated by a dotted line). The normalized heater signal, u_{HT}, is selected between 0 (off) and 1 (on with nominal power). The sample time of the power controller was set to $\Delta t_s = 3\,\mathrm{s}$. The third subplot shows the mean system temperature, T_{Mean}, and the component temperatures T_{CS}, T_{PS}, and T_{HM}. The state of charge of the battery, SOC, is shown in the fourth subplot. The terminal conditions, $T_{Mean}(t_f) = T^f = 50°\mathrm{C}$ and $\mathrm{SOC}(t_f) = \mathrm{SOC}^f = 0.7$,

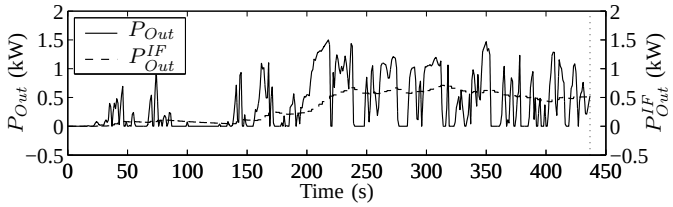

(a)

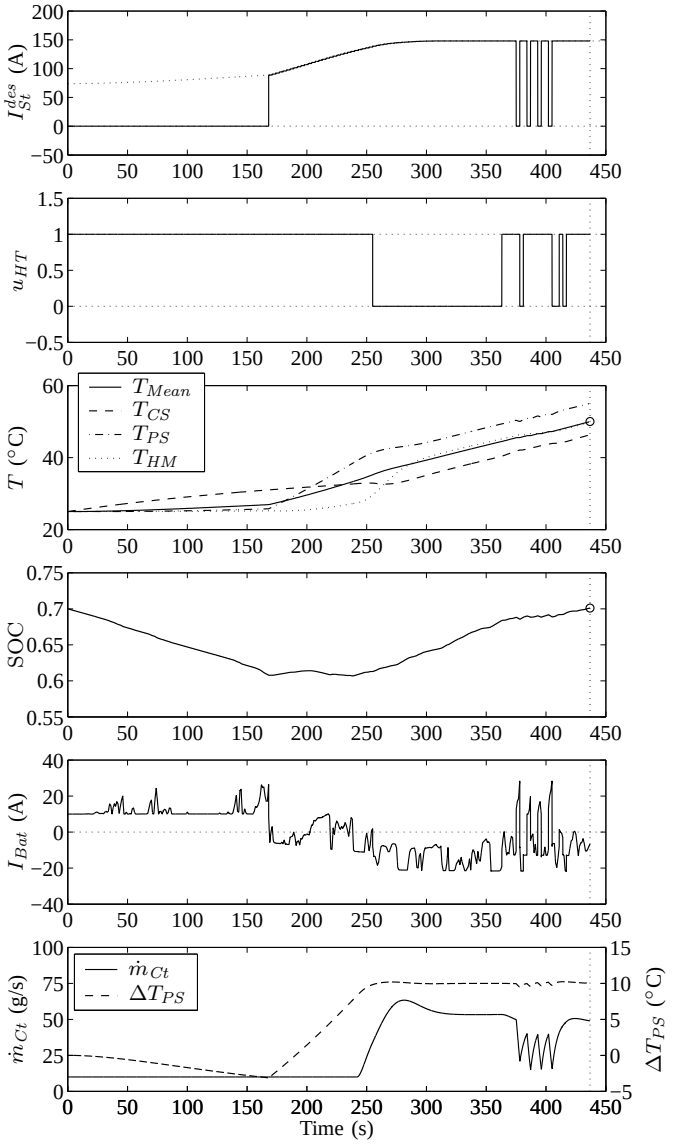

(b)

Fig. 8. Simulation results for an optimally controlled system warm-up: (a) power demand signal and output signal of the controller input filter (the remaining inputs were set to be constant, $\lambda_{Air}^{des} \equiv 2$, $T_{Amb} \equiv 25°\text{C}$, $T_{mAir}^{HM\,In} \equiv 20°\text{C}$, $T_{mH_2}^{PS\,In} \equiv 40°\text{C}$), (b) control signals and resulting state trajectories and output trajectories.

are each identified by a circle. In subplot 5 the battery current, I_{Bat}, is plotted. Positive values mean discharging of the battery, negative values indicate charging. The last subplot of Fig. 8(b) shows the input signal ΔT_{PS} and the control signal $\dot{m}_{Ct}$ of the coolant flow controller. The maximum temperature gap over the power section was set to $\Delta T_{PS}^{max} = 10°\text{C}$, and the minimum coolant mass flow rate was defined as $\dot{m}_{Ct}^{min} = 10\,\text{g/s}$. The fan signal u_{Fan} is equal to zero. All controller parameters correspond to the values given in Table II.

Despite the erratic power demand, the power controller switches the output signals only a few times. This behavior is a direct consequence of the averaging of the power demand at the controller input and of the discrete controller operation. However, the predefined state of charge of the battery is reached exactly at the end of the warm-up phase (charge sustainment), which is defined to be completed when the terminal temperature is reached. In the example shown in Fig. 8, a warm-up time of 437 s results (indicated by a dotted vertical line). At the beginning of the warm-up, the heater is on and the power is drawn from the battery. Consequently, the temperature of the system (specifically the temperature of the cooling system) rises and the state of charge of the battery decreases. After approximately 170 s the fuel cell stack is turned on to generate maximum electric power. The surplus power recharges the battery and the waste heat of the stack causes an increased heat flow to the system. Towards the end of the warm-up, the controller toggles the control signals to compensate for prediction errors. The coolant controller regulates the coolant mass flow rate as expected. When the heat generation inside the power section is small, the coolant mass flow rate is at its minimum value. Once the maximum tolerated temperature difference is reached, the controller increases the mass flow rate accordingly. Temperature offsets of less than 0.5°C are observed.

VI. Conclusion

A control-oriented mathematical model of the transient behavior of a hybrid fuel cell power system with auxiliary heater has been introduced. On the thermal part, it differentiates four component temperatures, namely the temperature of the power section, the temperature of the humidification section, and two temperatures of the cooling system. On the electric part, it models the fuel cell polarization, the power converter, and the battery with its state of charge. Due to the modeling approach based on physical principles there are only a few experiments necessary for the parameter identification. Hence, the model is applicable to different systems with little effort. The thermal part of the model and the polarization were validated against experimental data. Dynamic as well as static phenomena are reproduced accurately. From this model, a simplified version was derived to be used for the controller design. The reduced-order model constitutes a nonlinear, second-order system, which was shown to properly reproduce the mean system temperature and the state of charge of the battery.

The aim of minimizing the system warm-up time subject to a terminal state-of-charge constraint, which enables the charge-sustaining operation, has been transcribed into an optimal control problem formulation. A solution to this problem was derived from the necessary conditions of Pontryagin's Minimum Principle. The careful statement of simplifications and assumptions and the appropriate combination of the conditions for optimality allowed the formulation of the optimal

solution in a feedback manner. Besides algebraic calculations, the controller has to compute the zero of an integral equation to determine the optimal output signals. Due to its simple structure this controller is suited to be applied on-line. Moreover, its application to different systems should be feasible with minor effort, as its design is model-based. The optimal power controller, which controls the heater operation and the electrical current of the stack, was extended with a coolant controller. The coolant controller limits the spatial temperature gradient of the power section.

For various operating conditions and a set of controller parameters the optimal performance values of the controlled system has been compared with the solutions obtained with a direct feedforward method. The results confirmed the optimality of the control system derived. The relative performance losses, which mainly originate from the simplifications made during the controller design, amount to less than 2.4%. A simulated system warm-up demonstrated the functionality of the controller. As the optimal warm-up power controller accounts for cold-start transient power limitations of the fuel cell stack and determines the control signals subject to the model-based prediction, the predefined terminal constraints are exactly met. Simultaneously, a short system warm-up time to full power results. Compared to a system without battery nor auxiliary heater, the simulation showed a warm-up time reduced by 91% for the optimally controlled configuration proposed.

Further applications for the model and the optimization results gained throughout the course of this project are likely. The model should be readily employable for general thermal transient simulations, parameter investigations, state estimation, or model-based temperature controller designs. Equally, the direct feedforward optimization could be used for system parameter optimizations, as for example to determine the optimal size of the battery or of cooling system components.

ACKNOWLEDGMENT

The authors like to thank Denise McKay, Arlette Schilter, and also Daniel Ambühl for their contributions to this project.

REFERENCES

[1] P. Rodatz, G. Paganelli, A. Sciarretta, and L. Guzzella, "Optimal power management of an experimental fuel cell/supercapacitor-powered hybrid vehicle," *Control Engineering Practice*, vol. 13, no. 1, pp. 41–53, Jan. 2005.

[2] I. Arsie, C. Pianese, A. Di Domenico, and M. Sorrentino, "Transient analysis of PEM fuel cell for hybrid vehicle application," in *Proc. ASME Third International Conference on Fuel Cell Science, Engineering and Technology*, Ypsilanti, MI, 2005.

[3] K. S. Jeong, W. Y. Lee, and C. S. Kim, "Energy management strategies of a fuel cell/battery hybrid system using fuzzy logics," *Journal of Power Sources*, vol. 145, no. 2, pp. 319–326, Aug. 2005.

[4] J. C. Amphlett, R. F. Mann, B. A. Peppley, P. R. Roberge, and A. Rodrigues, "A model predicting transient responses of proton exchange membrane fuel cells," *Journal of Power Sources*, vol. 61, no. 1-2, pp. 183–188, 1996.

[5] J. H. Lee and T. R. Lalk, "Modeling fuel cell stack systems," *Journal of Power Sources*, vol. 73, no. 2, pp. 229–241, June 1998.

[6] X. Xue, J. Tang, A. Smirnova, R. England, and N. Sammes, "System level lumped-parameter dynamic modeling of PEM fuel cell," *Journal of Power Sources*, vol. 133, no. 2, pp. 188–204, June 2004.

[7] Y. J. Zhang, M. G. Ouyang, Q. C. Lu, J. X. Luo, and X. H. Li, "A model predicting performance of proton exchange membrane fuel cell stack thermal systems," *Applied Thermal Engineering*, vol. 24, no. 4, pp. 501–513, Mar. 2004.

[8] E. A. Müller and A. G. Stefanopoulou, "Analysis, modeling, and validation for the thermal dynamics of a polymer electrolyte membrane fuel cell system," *Journal of Fuel Cell Science and Technology*, to be published.

[9] D. D. Boettner, G. Paganelli, Y. G. Guezennec, G. Rizzoni, and M. J. Moran, "Proton exchange membrane fuel cell system model for automotive vehicle simulation and control," *Journal of Energy Resources Technology*, vol. 124, no. 1, pp. 20–27, Mar. 2002.

[10] K. Wipke, M. Cuddy, D. Bharathan, S. Burch, V. Johnson, A. Markel, and S. Sprik, "Advisor 2.0: A second generation advanced vehicle simulator for systems analysis," National Renewable Energy Laboratory (NREL), Tech. Rep., Mar. 1999.

[11] M. Athans and P. L. Falb, *Optimal Control: An Introduction to the Theory and Its Applications*. New York: McGraw-Hill, 1966.

[12] J. Chiasson and B. Vairamohan, "Estimating the state of charge of a battery," *IEEE Trans. Contr. Syst. Technol.*, vol. 13, no. 3, pp. 465–470, May 2005.

[13] *GESOP Software User Manual*, GESOP SUM 4.6.0, Institute of Flight Mechanics and Control, University of Stuttgart, Feb. 2004.

Eric A. Müller was born in Uster, Switzerland, in 1977. He received the Diploma in Mechanical Engineering in 2002 from the Swiss Federal Institute of Technology (ETH) Zurich, Switzerland.

Since 2002, he has been working as a Doctoral student at the Measurement and Control Laboratory at ETH Zurich. His research interests include modeling and optimal control of thermal systems, especially for automotive applications.

PLACE PHOTO HERE

Anna. G. Stefanopoulou Anna G. Stefanopoulou obtained her Diploma (1991, Nat. Tech. Univ. of Athens, Greece), M.S. (1992, Univ. of Michigan, U.S.) in Naval Architecture and Marine Engineering and her Ph.D. (1996, Univ. of Michigan) in Electrical Engineering and Computer Science. Dr. Stefanopoulou is presently an Associate Professor at the Mechanical Engineering Department at the University of Michigan. She was an Assistant Professor (1998-2000) at the University of California, Santa Barbara, and a Technical Specialist (1996-1997) at the Scientific Research Laboratories at Ford Motor Company. Her current research interests are in control of advanced internal combustion engines and fuel cell power systems.

Lino Guzzella was born in Zurich, Switzerland in 1957. He received the Diploma in Mechanical Engineering in 1981 and the Dr. sc. techn. degree in Control Engineering in 1986 from the Swiss Federal Institute of Technology (ETH) Zurich.

From 1987 to 1989 he was with the R&D-Department of Sulzer Bros. in Winterthur, Switzerland. From 1989 to 1991 he was an Assistant Professor for Automatic Control in the Electrical Engineering Department of ETH Zurich. He then joined Hilti R&D, Liechtenstein where he was the head of the Mechatronics Department from 1992 to 1993.

He is currently Professor for Thermotronics in the Mechanical Engineering Department of ETH Zurich. His research interests are modeling and optimization of dynamic systems, non-linear and robust control and applications of these ideas to thermal and especially automotive systems.

CONTENTS